Int. J. Heat Mass Transfer. Vol. 15, pp. 1001–1021. Pergamon Press 1972. Printed in Great Britain

VERY HIGH TEMPERATURE LAMINAR FLOW OF A GAS THROUGH THE ENTRANCE REGION OF A COOLED TUBE—NUMERICAL CALCULATIONS AND EXPERIMENTAL RESULTS*

LLOYD H. BACK

Jet Propulsion Laboratory, California Institute of Technology, Pasadena, California, U.S.A.

(*Received* 4 *September* 1970 *and in revised form* 11 *August* 1971)

Abstract—The laminar flow equations in differential form are solved numerically on a digital computer for flow of a very high temperature gas through the entrance region of an externally cooled tube. The solution method is described and calculations are carried out in conjunction with experimental measurements. The agreement with experiment is good, with the result indicating relatively large energy and momentum losses in the highly cooled flows considered where the pressure is nearly uniform along the flow and the core flow becomes non-adiabatic a few diameters downstream of the inlet. The effects of a large range of Reynolds number and Mach number (viscous dissipation) are also investigated.

NOMENCLATURE

c_p', specific heat at constant pressure;
D, channel diameter;
f, any variable, equations (A.3)–(A.15);
H', static enthalpy;
H_w, wall to total enthalpy ratio, $H_w = \frac{H_w'}{H_{t_i}'}$;
H_t', stagnation enthalpy, $H_t' = H' + \frac{(w')^2 + (u')^2}{2}$;
I, first ionization potential;
I_m, I_M, I_H, mass, momentum and enthalpy integrals, equations (14) and (18);
J, number of iterations;
k', thermal conductivity or radial mesh factor, equation (A.1);
$\dot{m}$, mass flow rate;
M, Mach number or number of radial increments;
p', static pressure;
Pr, Prandtl number;
P, pressure parameter, $p_i'/\rho_i'(w_i')^2$;
q', heat flux, $q' = -k' \frac{\partial T'}{\partial r}$;
Q, dimensionless wall heat flux, $Q = \frac{q_w'}{(H_{t_i}' - H_w')} \frac{DPr}{\mu_i'}$;
r, radial increments;
r_w, tube radius;
Re_i, Reynolds number based on radius, $Re_i = \frac{\rho_i' w_i' r_w}{\mu_i'}$;
Re_{D_i}, Reynolds number based on diameter, $Re_{D_i} = \frac{\rho_i' w_i' D}{\mu_i'}$;
T', static temperature;
T_t', stagnation temperature;
u', radial velocity component;

* This work presents the results of one phase of research carried out in the Propulsion Research and Advanced Concepts Section of the Jet Propulsion Laboratory, California Institute of Technology, under Contract NAS7-100, sponsored by the National Aeronautics and Space Administration.

w', axial velocity component;
z, axial distance;
α, degree of ionization;
γ, specific heat ratio;
δ, velocity boundary layer thickness;
δ_t, thermal boundary layer thickness;
ϵ, tolerance, equation (A.15);
ζ, dimensionless radial distance,

$$\zeta = \frac{r}{r_w};$$

$\Delta\zeta_M$, radial increment at wall;
K, flow speed parameter,

$$K = \frac{(w_i')^2}{H_{t_i}};$$

μ', viscosity;
ξ, dimensionless axial distance,

$$\xi = \frac{z}{r_w};$$

Ξ, dimensionless axial coordinate,

$$\Xi = \frac{z}{D}\frac{1}{Re_{D_i}}\frac{1}{Pr};$$

ρ', density;
σ, weighing factor, equation (A.10);
τ', shear stress,

$$\tau' = \mu'\frac{\partial w'}{\partial r};$$

Υ, temperature parameter,

$$\Upsilon = \frac{c_p' T_i'}{H_{t_i}'};$$

ω, exponent of viscosity–temperature relation.

Subscripts

e, condition at edge of boundary layer;
i, inlet condition at centerline;
$0, \mathfrak{L}$, condition along channel centerline;
w, condition at channel wall;
$()_{m,n}$, quantity at mth radial and nth axial grid point.

Superscripts

$()'$, dimensional quantity;
$()^j$, jth interate;
$\bar{()}$, average value across or along flow.

I. INTRODUCTION

THIS study was undertaken to acquire a better understanding of the actual flow field and thermal environment in a very high temperature gas flow through a channel. Of particular importance in such a flow that may be found in devices used in propulsion systems and in high temperature research facilities is the determination of the heat transfer to the channel wall which often requires external cooling to remain intact. In general the calculation of heat transfer depends upon the knowledge of many factors such as the flow field, flow regime, i.e. laminar, transitional or turbulent, thermodynamic state of the gas, reaction rates, transport properties; and in electrical propulsion devices, on the presence of electric and magnetic fields and their interactions. The flow and thermal fields are consequently rather complex and not well understood in many devices.

In this paper laminar flow through an externally cooled tube is considered. Whereas flows through tubes are usually turbulent in most applications, in many very high temperature gas flows at moderate pressures this is not the case since the Reynolds numbers are low enough so that the flow is laminar, e.g. below about 2000. This situation is found in practice because the density is relatively low and the viscosity is relatively high and consequently viscous forces become increasingly more important relative to inertia forces. In these relatively low Reynolds number flows both the velocity and thermal boundary layers grow rather rapidly along the tube for nearly uniform conditions at the inlet, and the core flow may become non-adiabatic a few diameters downstream of the inlet. Other features of these flows in which the core flow temperature

might exceed the cooled wall temperature by a factor of 25 [1] are the large property variation across the flow, more than an order of magnitude, and the large velocity and temperature gradients in the wall vicinity [2]. The steepness of the velocity and temperature profiles in the vicinity of the cooled wall is an important aspect in the numerical calculation of such flows since the shear stress and the heat flux at the wall, proportional to these gradients, become difficult to determine accurately from the finite difference calculations. Conventional finite difference techniques with a fixed radial increment commonly used in a computer program to calculate essentially constant property tube flows or with wall heating [3, 4] or severe wall cooling [5], become too lengthy with an appreciable amount of wall cooling. The radial increments must be made too small in order to obtain sufficient detail in the wall vicinity to establish gradients accurately.

The laminar flow equations in differential form that are believed to be appropriate in the entrance region are solved numerically on a digital computer for flow of a monatomic gas at very high temperatures, but below those temperatures at which ionization [6] or radia-radiation effects become important. The important viscous stress and heat flux components considered are the shear stress in the axial direction and the radial heat flux. The analysis accounts for variable properties across the flow, radial convection and viscous dissipation. For internal flows without swirl and longitudinal wall curvature as considered herein, the assumption of uniform pressure across the flow that was made is believed to be satisfactory. An effort to appraise this assumption was made by including the radial momentum equation, but the numerical calculations were unstable.

The numerical calculations are carried out in conjunction with experimental results [1] to learn as much about the flow under consideration as possible and to determine the extent to which such flows are describable. The experiments were conducted with argon at inlet temperatures up to about 14000°R flowing through an externally cooled tube maintained at a temperature of 560°R. Static pressures and heat fluxes were measured along the tube wall and calorimetric probe measurements were obtained across the flow at an axial location. The Reynolds number based on diameter ranged from 450 to about 600; the tube length was about 14 radii, and the inlet Mach number was about 0·075.

The analysis and finite difference formulation are described first, the latter in Appendix A. The numerical calculations are then discussed and the results are compared to the experiments. After establishing confidence in the numerical calculations by virtue of their agreement with the experiments, the effects of a larger range of Reynolds number and Mach number (viscous dissipation) are investigated.

Although the intent of the paper is not to survey methods of calculating internal laminar flows, prior theoretical investigations are discussed in connection with the problem at hand since there is uncertainty in the appropriate method that should be used, and there is little experimental data available to appraise the variable property predictions that have been made. Moreover, although primary emphasis is placed on describing a calculation scheme best fitted to the problem at hand, there is also interest in briefly discussing the difficulties encountered in carrying out the calculations to provide information on the general calculation of internal laminar flows, especially those with large property variation.

II. ANALYSIS

For steady, axisymmetric, laminar flow the conservation equations that are taken to describe the flow in the entrance region of a tube are as follows:

continuity equation

$$\frac{\partial}{\partial z}(\rho' w') + \frac{1}{r}\frac{\partial}{\partial r}(r\rho' u') = 0 \qquad (1)$$

axial momentum equation

$$\rho' w' \frac{\partial w'}{\partial z} + \rho' u' \frac{\partial w'}{\partial r} = -\frac{dp'}{dz} + \frac{1}{r}\frac{\partial}{\partial r}\left(r\mu' \frac{\partial w'}{\partial r}\right) \quad (2)$$

total energy equation

$$\rho' w' \frac{\partial H_t'}{\partial z} + \rho' u' \frac{\partial H_t'}{\partial r} = \frac{1}{r}\frac{\partial}{\partial r}\left(rk' \frac{\partial T'}{\partial r}\right) + \frac{1}{r}\frac{\partial}{\partial r}\left(rw'\mu' \frac{\partial w'}{\partial r}\right). \quad (3)$$

In these equations where the primes refer to dimensional quantities, w' and u' are the axial and radial velocity components in the z and r direction, respectively and the total enthalpy is

$$H_t' = H' + \frac{(w')^2 + (u')^2}{2}.$$

In this form of the momentum and energy equations, the important viscous stress is taken to be the shear stress in the axial direction, $\tau' = \mu' \partial w'/\partial r$, the important heat flux that in the radial direction $q' = -k' \partial T'/\partial r$ and the pressure is taken to be uniform across the flow so that $p'(z)$. For the flow under consideration, i.e. Reynolds numbers of about 500 and larger and a Prandtl number of $\frac{2}{3}$ for non-ionized gases these considerations are expected to adequately describe the flow based on constant property calculations, e.g. see [7–10].

Independent variables are introduced as follows

$$\zeta = \frac{r}{r_w} \qquad \xi = \frac{z}{r_w}$$

so that the radial coordinate ζ is 0 at the centerline and 1 at the wall, and the axial distance is given in terms of tube radii r_w. The conservation equations are then made dimensionless with respect to inlet values at the centerline, i.e. $\xi = 0, \zeta = 0$ denoted by the subscript i,

$$w = \frac{w'}{w_i'}, \quad u = \frac{u'}{w_i'}, \quad H_t = \frac{H_t'}{H_{t_i}'}, \quad T = \frac{T'}{T_i'},$$

$$\rho = \frac{\rho'}{\rho_i'}, \quad p = \frac{p'}{p_i'}, \quad \mu = \frac{\mu'}{u_i'}$$

to give

$$\frac{\partial}{\partial \xi}(\rho w) + \frac{1}{\zeta}\frac{\partial}{\partial \zeta}(\zeta \rho u) = 0 \quad (4)$$

$$\frac{\partial w}{\partial \xi} = -\frac{u}{w}\frac{\partial w}{\partial \zeta} - \frac{P}{\rho w}\frac{dp}{d\xi} + \frac{1}{\rho w Re_i} \times \left\{\mu \frac{\partial^2 w}{\partial \zeta^2} + \left[\frac{\partial \mu}{\partial \zeta} + \frac{\mu}{\zeta}\right]\frac{\partial w}{\partial \zeta}\right\} \quad (5)$$

$$\frac{\partial H_t}{\partial \xi} = -\frac{u}{w}\frac{\partial H_t}{\partial \zeta} + \frac{\Upsilon}{\rho w Re_i Pr}\left\{\mu \frac{\partial^2 T}{\partial \zeta^2} + \left[\frac{\partial \mu}{\partial \zeta} + \frac{\mu}{\zeta}\right]\frac{\partial T}{\partial \zeta}\right\} + \frac{K}{\rho w Re_i}\left\{\mu\left[w\frac{\partial^2 w}{\partial \zeta^2} + \left(\frac{\partial w}{\partial \zeta}\right)^2\right] + \left[\frac{\partial \mu}{\partial \zeta} + \frac{\mu}{\zeta}\right] w \frac{\partial w}{\partial \zeta}\right\}. \quad (6)$$

The parameters in these equations, in addition to the Prandtl number $Pr = \mu' c_p'/k'$ refer to the inlet condition and are given by

$$\left.\begin{aligned} P &= \frac{p_i'}{\rho_i'(w_i')^2} = \frac{1}{\gamma M_i^2} \\ K &= \frac{(w_i')^2}{H_t'} = \frac{(\gamma - 1)M_i^2}{1 + \frac{\gamma - 1}{2} M_i^2} \\ \Upsilon &= \frac{c_p' T_i'}{H_{t_i}'} = \frac{1}{1 + \frac{\gamma - 1}{2} M_i^2} \\ Re_i &= \frac{\rho_i' w_i' r_w}{\mu_i'} \end{aligned}\right\} \quad (7)$$

Other relations that describe the flow under consideration are the perfect gas relation $p' = \rho' R T'$ which in dimensionless form is

$$p = \rho T \quad (8)$$

the viscosity–temperature relation $\mu'(T')$ which can be described empirically by the power law relation

$$\mu = T^{\omega} \quad (9)$$

and the total enthalpy which in dimensionless

form is

$$H_t = \Upsilon T + K\left(\frac{w^2 + u^2}{2}\right). \quad (10)$$

The parameters Υ and K, which are a measure of the thermal and kinetic energies in the inlet flow are interrelated, $1 = \Upsilon + K/2$, since $u_i = 0$ because of symmetry.

The following inlet and boundary conditions are considered. At the tube inlet the axial velocity and enthalpy distributions are prescribed and the radial velocity is taken to be zero, i.e.

$$\text{at} \quad \xi = 0: \quad \frac{w'}{w'_i} = w(\zeta), \quad \frac{H'_t}{H'_{t_i}} = H_t(\zeta), \quad u = 0. \quad (11)$$

The tube wall is taken to be impermeable and at a specified temperature dictated by external cooling so that the enthalpy at the wall is known, i.e.

$$\text{at} \quad \zeta = 1; \quad w = 0, \quad u = 0, \quad H = H_w(\xi). \quad (12)$$

Other boundary conditions along the wall could be treated as well, e.g. mass transfer cooling by including the diffusion equation too, or radiation cooling.

Along the centerline the radial velocity must vanish, and symmetry conditions give

$$\text{at} \quad \zeta = 0; \quad u = 0, \quad \frac{\partial w}{\partial \zeta} = 0, \quad \frac{\partial H_t}{\partial \zeta} = 0. \quad (13)$$

III. GENERAL CONSIDERATIONS AND PREVIOUS ANALYSES

Before describing the calculations some discussion of the treatment of internal flows is appropriate with regard to the form of the equations that are considered. The system of six equations (4)–(6) and (8)–(10) contain seven unknown quantities w, u, H_t, T, p, ρ and μ since the radial momentum equation has been essentially replaced by disregarding any pressure variation that may occur radially in a real flow. For internal flows without rotation and curved walls this assumption appears plausible for the Reynolds number range of this investigation. Nevertheless, in the early stages of this investigation the pressure was allowed to vary radially as well as axially, i.e. $p'(r, z)$ by including the following form of the radial momentum equation

$$\rho' w' \frac{\partial u'}{\partial z} + \rho' u' \frac{\partial u'}{\partial r} = -\frac{\partial p'}{\partial r} + \frac{\partial}{\partial z}\left(\mu' \frac{\partial w'}{\partial r}\right).$$

The numerical calculations however were unstable, in that pressure oscillations that were calculated across the flow increased in amplitude at subsequent axial stations. Similar difficulty in trying to include radial pressure variation across a flow was found by Baum and Dennison [11] in their numerical calculation of supersonic laminar wakes. Although the radial momentum equation was not included, the assumption of uniform pressure across the flow was thought to be satisfactory since the Reynolds numbers are not real low and the actual pressure variation across the flow is probably unimportant in the calculation of quantities of interest, e.g. wall heat flux and shear stress for the flows under consideration.

The mathematical form of the equations considered herein is not immediately clear; there apparently being one more unknown quantity than equation when the pressure is taken to be invariable across the flow. At first sight it would appear that one of the variables, preferably the pressure since it is measurable along the tube wall, should be specified in order to calculate the internal flow variables. Alternately, if radial convection were suppressed, i.e. $u = 0$, the equations would appear to be mathematically determinate, but there is no justification for such an *a priori* presumption that is known to lead to an overestimate of the predicted heat transfer. However, other numerical calculations have been carried out for the variable property form of the equations considered herein without specifying one of the variables, nor suppressing the radial velocity [3–5]. In particular, for the case of a constant

property, isothermal flow the three variables are the velocity components, w and u and the assumed uniform pressure across the flow $p(z)$; the two differential equations are those of continuity and axial momentum. Bodoia and Osterle [12] closed the system of equations by adding the integrated continuity equation across the flow as also was later done in [13]

$$\int_0^{r_w} \rho' w' r \, dr = \text{constant}.$$

Wendel and Whitaker [14] in commenting on the numerical calculations of Bodoia and Osterle suggest that the radial velocity is not actually being included. Closure of the system of equations by adding the integrated continuity equation has also been incorporated in subsequent heat transfer investigations in the inlet region of a tube for a constant property flow where the energy equation is an uncoupled part of the systems of equations, e.g. [15–18], or for a variable property flow where all the equations are coupled [3, 5]. Worsoe–Schmidt and Leppert [3] argue that for tube flows the pressure can only depend on axial velocity when the pressure is assumed uniform across the flow and therefore invoke the constraint that the mass flow be conserved as given by the integrated continuity. Other constraints have also been suggested, e.g. Sparrow, Lin and Lundgren [19] use the integrated axial momentum equation across the flow in their constant property flow field calculations. Diessler and Presler [4] propose another method in their investigation of uniform heating along a tube by application of the momentum equation along the tube wall where the velocity vanishes to specify the pressure at the next axial location $z + \Delta z$ from the pressure gradient term with the radial gradient of the shear evaluated at the z location.

It is difficult to judge the implication of those methods in which all the flow variables are calculated including the pressure when it is assumed uniform across the flow by invoking one of the various constraints previously mentioned. Clearly, if the radial momentum equation is retained the problem is tractable. For example, for constant property, isothermal flow the second order axial and radial momentum equations and first order continuity equation can be reduced to a set of five first order equations for the unknowns w, $\partial w/\partial r$, u, $\partial u/\partial r$ and $p(r, z)$. Correspondingly, there are five boundary conditions across the flow: two at the wall $w = 0$, $u = 0$ and three along the axis, $u = 0$, $\partial w/\partial r = 0$ and $\partial p/\partial r = 0$. The treatment of variable property flow just introduces the second order energy equation with two boundary conditions on H_t and other relations equations (8)–(10), thereby increasing the set of first order equations and boundary conditions to seven. However, when the radial momentum equation is deleted and the pressure is assumed uniform across the flow, i.e. $p(z)$, the set of first order equations is reduced by two, but the boundary conditions only by one, i.e. $\partial p/\partial r$ is redundant. Then perhaps, invoking the mass flow constraint is tantamount to utilizing the excess boundary condition that can only depend on z to effectively be able to calculate $p(z)$ since the mass flow constraint requires that the radial velocity vanish along the axis as well as along the wall, as can be seen by integrating the continuity equation (1) across the flow. However, the coupling between the conservation equations and boundary conditions is more complex and should require the satisfaction of the integral form of all the conservation equations (mass, momentum and energy) at each axial step. An attempt was made to satisfy these global relations at each axial step as described in Appendix B. However, in the method the calculated pressure varies across the flow, being incompatible with the assumption of uniform pressure across the flow implied in the equations that are being solved. Attempts to smooth out the calculated radial pressure variation at a given axial location by obtaining an average value across the flow $\bar{p}$ led to an unstable scheme since $\bar{p}$ would oscillate and increase in absolute magnitude with successive iterations. It is clear that if the pressure is to

be calculated a more approximate scheme is required that may not satisfy all of the integral constraints.

The point to be made is that there is uncertainty in the appropriate method that should be used to calculate internal flows, especially when properties are variable. Even for constant property flows not much information is available to appraise the calculations that have been made, e.g. see the comparison to internal flow measurements in [19] and heat transfer measurements in particular in [17] although other heat transfer measurements have been made, e.g. [20]. For variable property flows less information is available. The numerical calculations by Incropera and Leppert [5] that included the mass flow constraint were carried out for the case of a severely cooled tube $T'_w/T'_i = 0{\cdot}05$ and the calculations by Worsoe–Schmidt and Leppert [3] for the case of wall heating, T'_w/T'_i up to 5 and a moderately cooled tube, $T'_w/T'_i = 0{\cdot}5$. However, neither of these theoretical investigations contain comparisons to experimental data, nor are any predicted wall pressure distributions shown. Recent heat transfer measurements in [21] for a moderate amount of uniform wall heating, T'_w/T'_i up to about 2, were however, in reasonable agreement with the numerical predictions of [22] which are similar to those of Worsoe–Schmidt and Leppert [3]. But again pressure measurements were not indicated. The calculations by Deissler and Presler for uniform wall heating show a larger pressure drop in the inlet region than for constant property flow, but no experimental information was presented nor apparently is available to appraise their predictions.

These observations do reveal a need for a combined theoretical and experimental study with the latter involving both wall pressure and heat transfer measurements. In the majority of the calculations carried out herein the pressure was specified from wall pressure measurements. However solutions were also obtained where the pressure was also calculated: the particular method used is described in Section IV and compared to measurements in Section V.

The finite difference formulation is described in Appendix A.

IV. GLOBAL CONSIDERATIONS

Since there are errors in the finite difference approximations that depend upon the mesh size and there are numerical round off errors to a lesser extent, some method needs to be employed to insure that calculated values from the iteration scheme converge to the true values. Two methods were used: one in which the pressure was specified and in the other where it was calculated. For the flows discussed in Section V where the pressure distribution was prescribed from measurements, the continuity equation (1) was also satisfied on a global basis as it must be

$$I_{m_i} - I_m = 0 \quad \text{where} \quad I_m = \int_0^1 \rho w \zeta \, d\zeta. \tag{14}$$

This was accomplished by calculating new values of the axial velocity w across the flow that did satisfy the mass flow constraint after each iteration

$$w_{\text{corrected}} = w_{\text{computed}} \frac{I_{m_i}}{(I_m)_{\text{computed}}} \tag{15}$$

This scheme is self-corrective i.e. too large velocities are made smaller and vice versa, since the velocity is contained in the computed integral. These corrected velocities along with other variables were then used as the jth iterate to obtain the $j + 1$ iterate (Appendix A). The calculation then continues until convergence within the tolerance ϵ is achieved. By not invoking the mass flow constraint at each axial step, there was a progressive increase in the calculated mass flow rate along the tube that amounted to as much as 10 per cent for the experiments discussed in Section V where the pressure was nearly uniform.

In addition to satisfying the mass flow constraint the integral form of the conservation

equations (2) and (3) (i.e. momentum and energy) should be satisfied. In non-dimensional form these are

$$I_{M_i} - I_M = \tfrac{1}{2}P(p-1) + \int_0^{\xi} \tau_w \, d\xi \qquad (16)$$

$$I_{H_i} - I_H = \int_0^{\xi} q_w \, d\xi \qquad (17)$$

where the momentum and enthalpy integrals are

$$I_M = \int_0^1 \rho w^2 \zeta \, d\zeta; \qquad I_H = \int_0^1 \rho w H_t \zeta \, d\zeta \qquad (18)$$

and the non-dimensional wall shear stress and heat flux to the wall are

$$\tau_w = \frac{\tau'_w}{\rho'_i (w'_i)^2}; \qquad q_w = \frac{q'_w}{\rho'_i w'_i H'_{t_i}}. \qquad (19)$$

These relations are referred to in Section V, also in connection with momentum and energy losses in the flow. The integrals were evaluated by a fifth order quadrature technique with a fifth power error term.

It was possible to calculate the pressure distribution along the flow i.e. $p(z)$ by using the the mass flow constraint in conjunction with an averaged momentum equation involving a balance between the axial convective acceleration and pressure gradient. In this method, the pressure is adjusted so that the axial velocity is forced to satisfy the mass flow constraint. Mathematically this means that if

$$\int_0^1 \rho w \zeta \, d\zeta \neq I_{m_i}$$

then w was changed by setting

$$\int_0^1 \rho (w + \overline{\Delta w}) \zeta \, d\zeta = I_{m_i}.$$

Solving this relation for $\overline{\Delta w}$ at each axial step and relating this change in velocity to the change in pressure from the following form of the momentum equation

$$\overline{\Delta w} = -\frac{P \Delta p}{\overline{\rho w}} \quad \text{where} \quad \overline{\rho w} = \frac{\int_0^1 \rho w \zeta \, d\zeta}{\int_0^1 \zeta \, d\zeta}$$

gives the following expression for the change in pressure after each iteration

$$\Delta p = \frac{\int_0^1 \rho w \zeta \, d\zeta - I_{m_i}}{\frac{P}{\overline{\rho w}} \int_0^1 \rho \zeta \, d\zeta}.$$

This method has the advantage that if too large axial velocities are calculated to be compatible with the mass flow constraint then they are reduced by calculating a pressure rise and vice versa, so that the method converges in subsequent iterations. The actual Δp at each axial step is then obtained by adding the Δp's calculated at each iteration $\Delta p = \Sigma \Delta p_j$. Results from this method are discussed in Section V.

A brief discussion of other numerical approaches that were attempted appears in Appendix B.

V. NUMERICAL CALCULATION AND EXPERIMENTAL RESULTS

The numerical calculations are appraised by comparison with measurements of static pressure and heat flux along the wall of an externally cooled tube and with calorimetric probe and spectroscopic measurements across the flow at an axial location. The experimental conditions for the tests considered herein are shown in Table 1. For these measurements which are described in detail in [1] the effect of ionization was considered to have been comparatively small as indicated by the analysis of [6]. Thermal radiation from the gas to the wall was also considered to have been small as indicated by measurements with argon in [23] with a window covered cavity for which the contribution of the radiative heat flux to the wall did not exceed 1–2 per cent of the convective heat flux over a range of operating conditions that

Table 1. Experimental conditions for argon flow through a cooled tube $r_w = 0.975$ in.

	Test No.		
	51-H	59-H	63-H
H'_{ti}, Btu/lb	1760	1800	1280
H'_w/H'_{ti}	0·040	0·039	0·055
$Re_{D_i} = \frac{\rho'_i w'_i D}{\mu'_i}$	450	560	590
M_i	0·076	0·073	0·072
$\left(\frac{\alpha I}{H'_t}\right)_i$ Ionization energy fraction	0·017	0·019	0·0003
p'_{ti}, psia	4·20	5·93	4·09
$\dot{m}$, lb/s	0·00944	0·0126	0·0104
T'_{ti}, °R	13 900	14 200	10 300

span the experimental conditions considered herein (pressures from 1 to 6 psia, temperatures from 5600 to 17000°R enthalpies from 700 to 2400 Btu/lb and a highly cooled wall, $H_w \simeq 0{\cdot}05$). Confidence in the internal flow conditions was established by the good agreement between the average enthalpies determined from the probe data and the energy balance as well as the good agreement of the gas temperature determined from the probe data based on assumed equilibrium conditions and the excitation temperature determined from spectroscopic measurements of intensities of atom lines by the relative line intensity method [1]. The wall heat flux was determined by calorimetry in circumferential coolant passages. A very good check was found (within 1 per cent)

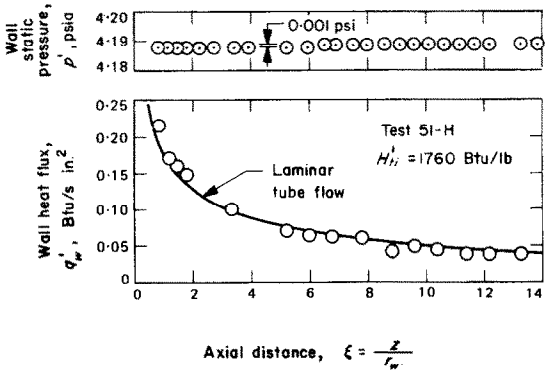

FIG. 1. Wall static pressure and heat flux distributions along the tube.

between the total heat load to the entire apparatus that was externally cooled and the applied power to the three arc heaters upstream from which the heated argon discharged radially into a plenum chamber. The mixed, high temperature gas was then accelerated through a short, bell mouth contraction section with a contraction area ratio of 5·3 before entering the tube. A choked nozzle was attached to the downstream end of the tube. The effect of free convection was not believed to be significant by inference from the good agreement between the calculated and measured wall heat fluxes that will be shown subsequently.

Pressures were measured along the length of the tube with 24 silicone oil manometers (specific gravity 0·93) that are believed to be accurate to a pressure difference of 0·001 psi. There appears to be a slight increase in pressure along the tube as indicated by the test shown in Fig. 1 (51-H) and this was also found for the other two tests (59-H and 63-H) where the rise amounted to 0·002 psi. This pressure rise however is small e.g. the pressure term $(\frac{1}{2})P(p-1)/I_{M_i}$ that appears in the integral form of the momentum equation (16) amounts to 0·025 at the end of the tube for test 51-H, and therefore a uniform pressure condition along the flow was utilized in the majority of the numerical calculations. In another investigation of a very high temperature gas flow through a cooled, rectangular

cross-sectional area channel [24], the pressure was also found to be essentially constant along the channel whose length was 40 hydraulic radii.

The nearly uniform pressure that is found in the entrance region of these very high temperature gas flows through cooled tubes is believed to primarily result from the negligible change in the effective core flow area because of shear layer development. As will be subsequently seen the mass flux in the shear layer is hardly

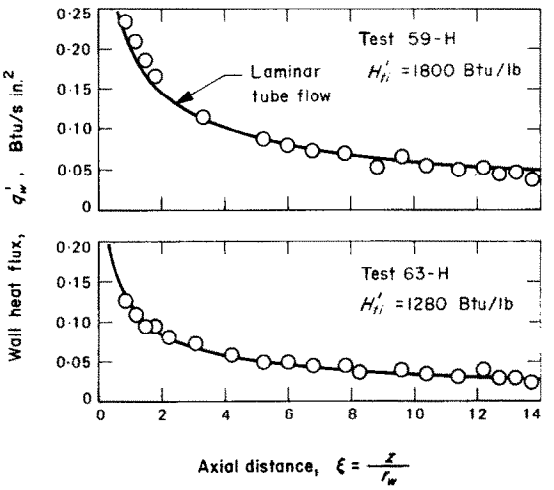

FIG. 2. Wall heat flux distributions along the tube at other conditions.

changed from its core flow value and therefore the displacement effect is small. This is unlike the situation found in tube flows with little or no heat transfer where pressure drop occurs as the core flow is accelerated by virtue of the mass flux deficit in the shear layer.

The contraction section preceding the tube is believed to have produced a nearly uniform flow with a relatively thin boundary layer from which the numerical calculations were initiated by assuming uniform axial velocity and enthalpy profiles there. Appendix C contains a discussion of the numerical parameters used in the calculations. The results which were obtained by using the following properties for argon with negligible ionization $Pr = \frac{2}{3}$, $\omega = \frac{3}{4}$, $\gamma = \frac{5}{3}$ are discussed in this section.

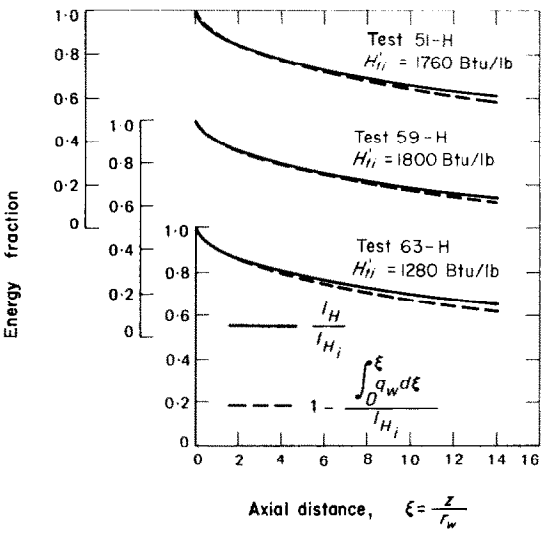

FIG. 3. Energy fractions along the tube.

The heat flux to the tube wall, the important result which governs the cooling requirements and energy loss from the flow, is shown in Fig. 1 for test 51-H. The numerical predictions are seen to be in excellent agreement with the measured heat fluxes along the tube, and this correspondence applies as well to the two other tests 59-H and 63-H, at somewhat different inlet conditions, that are shown in Fig. 2. The energy loss to the wall is relatively large in the flows considered as indicated in Fig. 3 by the fraction of energy remaining in the flow at any axial location. By the end of the tube about 40 per cent of the energy in the inlet flow was

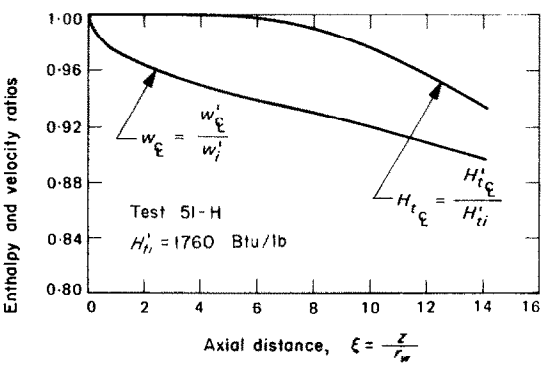

FIG. 4. Centerline velocity and enthalpy distributions along the tube.

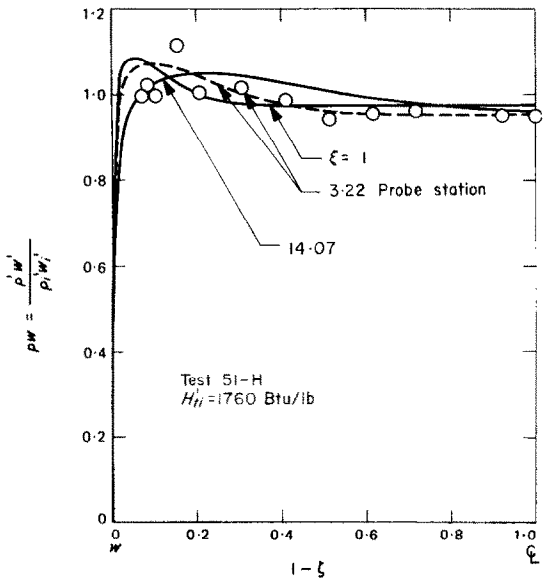

FIG. 5. Many flux profiles across the flow.

lost by heat transfer to the tube wall. The difference between the solid and dashed curves shown in Fig. 3 indicate the degree to which the overall energy balance given by equation (17) is satisfied by the numerical calculations. Although this check is not precise, the agreement is considered to be satisfactory for the very high temperature flows considered.

The centerline distributions of velocity and enthalpy along the tube are shown in Fig. 4 for test 51-H. Immediately downstream of the inlet the centerline velocity begins to decrease and the flow decelerates there presumably because of the relatively large amount of wall cooling that causes the mass flux in the wall region to exceed the centerline value. This is seen in Fig. 5 where the radial distributions of mass flux are shown. To satisfy the mass flow constraint, the mass flux and thus the velocity in the center portion of the tube decreases below the inlet value as can be observed in Fig. 6 where the velocity profiles are shown. However, the thermal penetration is considerably less in the inlet region (Fig. 4) and the centerline enthalpy is not reduced by some prescribed amount, say 1 per cent, below the inlet value until a distance of 8 tube radii is reached. Farther downstream both the centerline velocities and enthalpies decrease, and if the calculations were extended to distances beyond the actual length of the tube, as they were, the centerline enthalpy

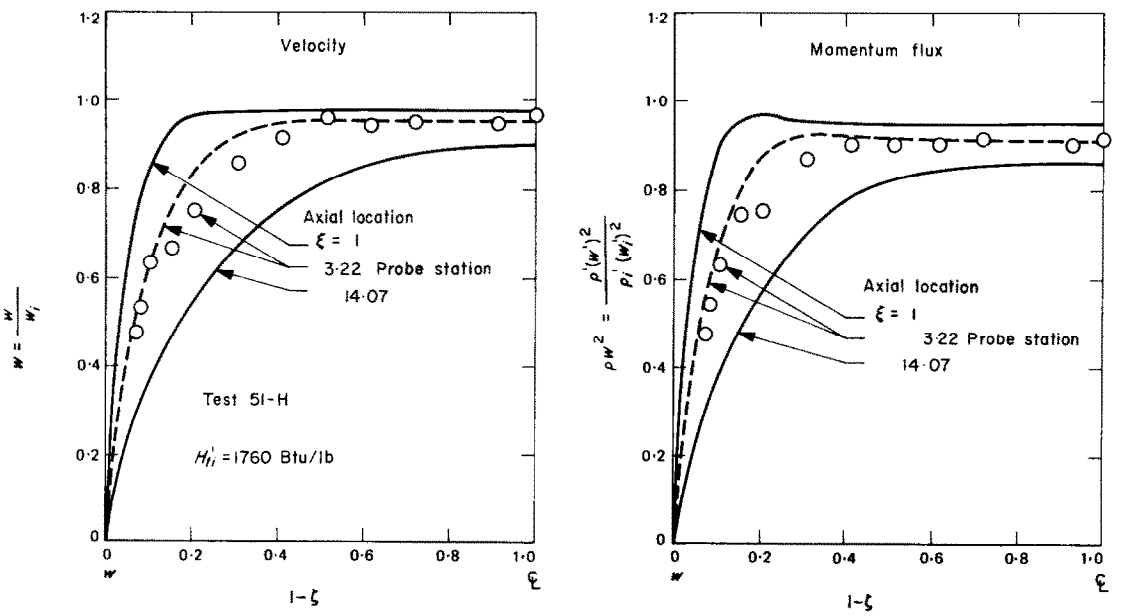

FIG. 6. Velocity and momentum flux profiles across the flow.

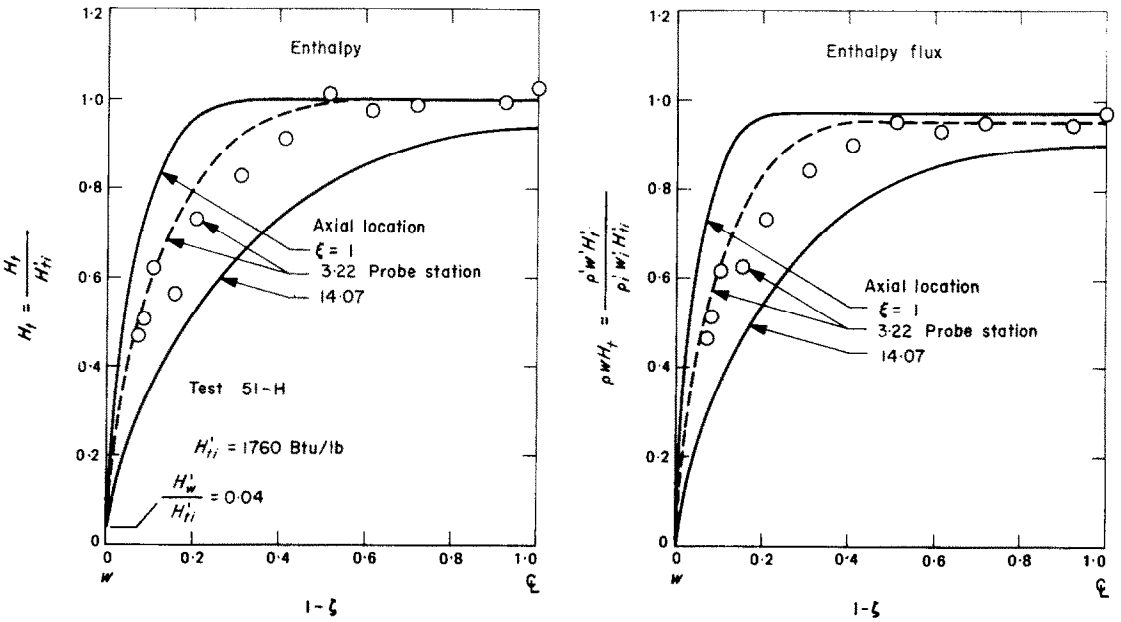

FIG. 7. Enthalpy and enthalpy flux profiles across the flow.

actually decreases more rapidly than the axial velocity i.e. the curves cross one another at ξ of about 22.

The progressive development of the flow and thermal distributions that are shown in Figs. 5–7 for test 51-H indicate the change of these distributions from their uniform values at the inlet. The slopes of these profiles become successively smaller near the wall in a way not basically different from that found for boundary layer growth over a surface, although in the inlet region the velocity in the center portion of the flow is reduced below its inlet value while the enthalpy remains the same. There is generally good agreement between the predicted profiles and probe measurements at $\xi = 3{\cdot}22$. At the end of the tube, $\xi = 14{\cdot}07$, both the flow and thermal penetrations are appreciable. As mentioned before the calculations were carried out to a larger value of $\xi = 40$, and in this vicinity there appeared to be the onset of a region of fully developed flow in the sense proposed by Mirels [25] for a low speed, high temperature gas flow through a highly cooled channel i.e. that the velocity and enthalpy profiles become similar across the flow when normalized by their local centerline values. The momentum flux profiles (Fig. 6) like the enthalpy flux profiles (Fig. 7) indicate the progressively larger momentum defect in the flow caused by the wall shear stresses. In this regard the momentum losses are similar to the energy losses

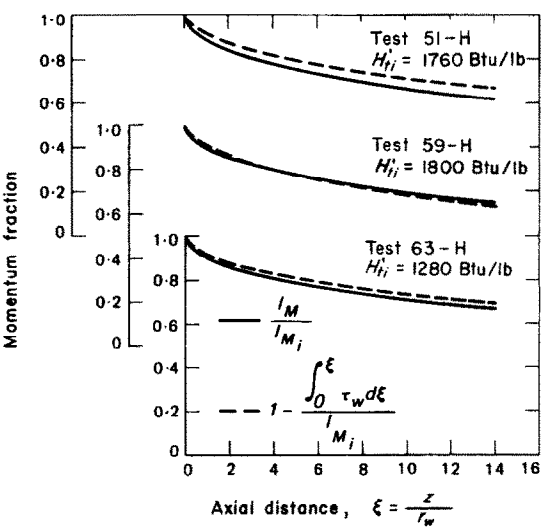

FIG. 8. Momentum fractions along the tube.

as seen in Fig. 8 where the momentum fractions are shown. Again the overall check on the momentum balance, equation (16) is considered to be satisfactory for the kind of flow considered.

Having found good agreement between the predictions and experiments, attention is focused on the more general question of how to represent the predictions over a range of conditions so that they can be utilized to indicate the influence of the various parameters. The choice in this regard is based on consideration of a simpler constant property, low speed form of the energy equation for a uniform flow that then involves only a balance between axial convection of energy by the mean flow and radial heat conduction. The change in the enthalpy profiles across the flow then depends upon the non-dimensional axial coordinate

$$\Xi = \frac{z}{D}\frac{1}{Re_{D_i}}\frac{1}{Pr} \tag{20}$$

as also do the non-dimensional wall heat fluxes or Nusselt numbers obtained from the slope of the enthalpy profiles at the wall

$$Q = \frac{q'_w}{(H'_{t_i} - H'_w)}\frac{DPr}{\mu'_i} \tag{21}$$

The non-dimensional wall heat flux distributions along the tube are shown in terms of Q and Ξ in Fig. 9. In the initial portion of the entrance region the tube flow predictions approach the solutions from a laminar boundary layer analysis. From [2] the laminar boundary layer prediction for low speed flow is of the form

$$\frac{q'_w}{(H'_{t_i} - H'_w)\,\rho'_i w'_i}\left(\frac{\rho'_i w'_i z}{\mu'_i}\right)^{\frac{1}{2}} Pr^{\frac{1}{3}} = A\left(\omega, Pr, \frac{H'_w}{H'_{t_i}}\right).$$

Translation of this prediction to the representation of Fig. 9 gives

$$\frac{q'_w}{(H'_{t_i} - H'_w)}\frac{DPr}{\mu'_i} = \left(\frac{A}{Pr^{\frac{1}{2}}}\right)\left(\frac{z}{D}\frac{1}{Re_{D_i}}\frac{1}{Pr}\right)^{-\frac{1}{2}}. \tag{22}$$

This prediction is shown in Fig. 9 for the values of wall cooling i.e. H_w/H_{t_i} indicated: for a larger range of wall cooling, values of $A/Pr^{\frac{1}{2}}$ are given in Table 2. In the inlet region the tube

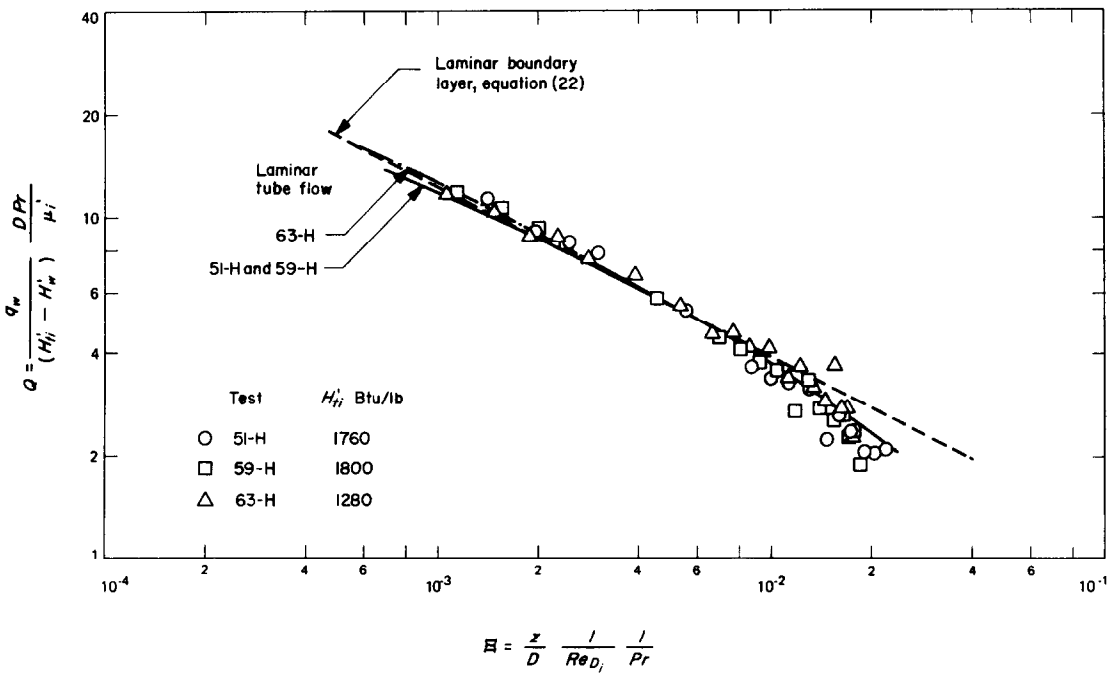

FIG. 9. Correlation of heat transfer results.

flow predictions are in close agreement with the boundary layer prediction and the experimental data. There is a tendency for the tube

Table 2. Variable property laminar boundary layer predictions with wall cooling; low speed flow, $\omega = \frac{3}{4}$, $Pr = \frac{2}{3}$

$\frac{H'_w}{H'_{ti}}$	0·01	0·04	0·2	0·6	1·0
A	0·367	0·364	0·354	0·339	0·329
$\frac{A}{Pr^{\frac{1}{3}}}$	0·393	0·389	0·379	0·363	0·352

flow predictions to approach the boundary layer prediction from below in the inlet region and this is believed to be caused by an underestimate of the actual slopes of the enthalpy profiles at the wall immediately downstream of the inlet where the enthalpy profiles are very steep near the wall. This apparently occurs in spite of using the small radial mesh spacing and extrapolation procedures described in Appendix A for obtaining the slopes of the profiles at the wall. The difference may also be attributable to some extent to flow deceleration which occurred in the inlet region. Farther downstream the thermal penetration extends to the centerline and the driving potential for heat transfer is less than the difference $(H'_{t_i} - H'_w)$ just downstream of the tube inlet. Consequently, the boundary layer prediction overestimates the heat transfer and agreement with the experimental data is afforded by the tube flow prediction.

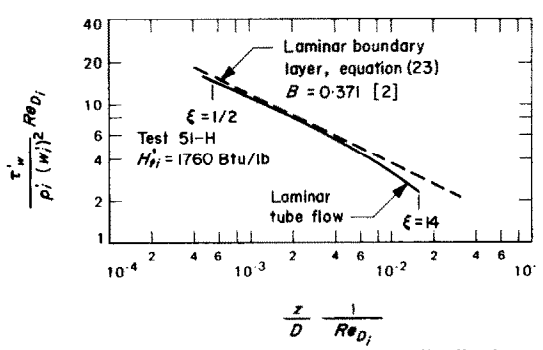

FIG. 10. Non-dimensional wall shear stress distribution.

A similar representation for the wall shear stress distribution is shown in Fig. 10. The laminar boundary layer prediction for low speed flow [2]

$$\frac{\tau'_w}{\rho'_i(w'_i)^2}\left(\frac{\rho'_i w'_i z}{\mu'_i}\right)^{\frac{1}{2}} = B\left(\omega, \frac{H'_w}{H'_{t_i}}\right)$$

when translated to the representation of Fig. 10 is

$$\frac{\tau'_w}{\rho'_i(w'_i)^2} Re_{D_i} = B\left(\frac{z}{D}\frac{1}{Re_{D_i}}\right)^{-\frac{1}{2}} \tag{23}$$

The behavior of the tube flow prediction relative to the boundary layer prediction is very similar to that found for the non-dimensional heat flux; however, it always lies below the boundary layer prediction because the velocity in the center portion of the tube in the inlet region is diminished because of wall cooling.

Application of the method described in Section IV to test 51-H to calculate the pressure distribution as well yielded a predicted pressure rise along the tube from the first pressure tap at $\xi = 0{\cdot}8$ to the last tap at $\xi = 13{\cdot}8$ that amounted to

$$\Delta p_{1-2} = \Sigma\Delta p = \frac{\Delta p'_{1-2}}{p'_i} = 0{\cdot}00054$$

or

$$\Delta p'_{1-2} = 0{\cdot}0023 \text{ psi.}$$

However, for this test the measured pressure rise of 0·001 psi was less (Fig. 1), although the discrepancy would be smaller for the other tests (59-H and 63-H) where the measured pressure rise was 0·002 psi. Because of the predicted pressure rise the overall check on the momentum balance equation (16) yielded lower values for the term

$$1 - \frac{\int_0^{\xi} \tau_w \, d\xi}{I_{M_i}} - \frac{1}{2}\frac{P(p-1)}{I_{M_i}}$$

than shown in Fig. 8 for test 51-H for the case

of a nearly uniform pressure: the values so obtained near the end of the tube were about one-half as much below those for I_M/I_{M_i} (solid curve) as the values for a uniform pressure were above (dashed curve). The centerline velocities were higher (Fig. 4) but the difference was small amounting to no more than 1 per cent by the end of the tube; the distribution along the tube being similar in shape to that shown in Fig. 4 for the uniform pressure case. The overall energy balance equation (17) differed only slightly from that shown for the uniform pressure case (Fig. 3) and the centerline enthalpies were virtually the same (Fig. 4). Both the predicted wall shear stress and heat flux were

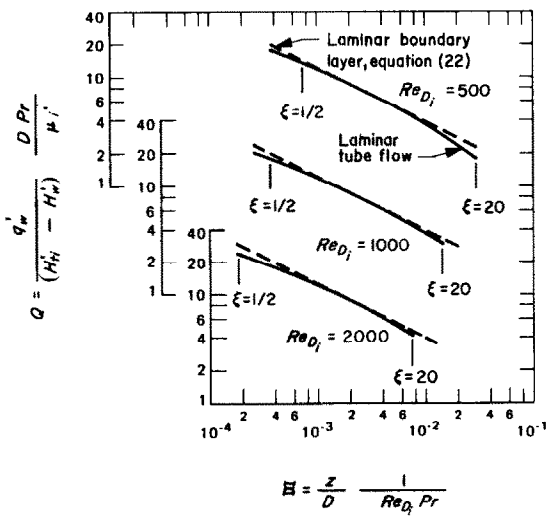

FIG. 11. Effect of Reynolds number on the non-dimensional wall heat flux distribution: $Pr = \frac{2}{3}$, $\omega = \frac{3}{4}$, $\gamma = \frac{5}{3}$, uniform inlet profiles, $M_i = 0{\cdot}1$, constant pressure, $H_w = 0{\cdot}04$, ξ to 20.

within 3 per cent of those obtained for the uniform pressure case, and consequently, at least for the experimental conditions herein, there is little difference in the wall friction and heat transfer predicted from either method of calculation.

Since the range of Reynolds numbers spanned by the experimental data is not large, an appraisal of the effect of Reynolds number on the non-dimensional heat flux Q in the Ξ representation is shown in Fig. 11. In the region where the predictions overlap one another in Ξ, the tube flow predictions virtually coincide with each other, thus indicating the utility of the representation shown. In these calculations the pressure was taken to be constant along the tube. This coincidence is also indicated by a different choice of dimensionless independent and dependent variables [3] than used herein, for the situation where the contribution of the radial velocity component to the kinetic energy in the stagnation enthalpy expression (nomenclature) is negligible i.e.

$$\frac{(u')^2}{2} \ll \frac{(w')^2}{2}.$$

This is usually the case unless the Reynolds number is relatively small.

For the range of Mach numbers considered (viscous dissipation) the non-dimensional heat flux shown in Fig. 12 is scarcely influenced. The tube flow prediction at the larger Mach number of 0·75 lies just barely below the lower Mach number prediction of 0·1. The flow speed parameter K was 0·32 for the higher Mach number inlet condition of 0·75 and this corresponds to a ratio of kinetic energy to total enthalpy of 0·16, a value however, that is not very large. The

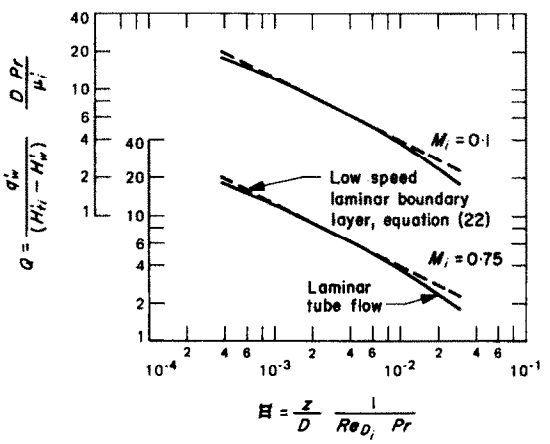

FIG. 12. Effect of Mach number (viscous heating) on the non-dimensional wall heat flux distribution: $Pr = \frac{2}{3}$, $\omega = \frac{3}{4}$, $\gamma = \frac{5}{3}$, uniform inlet profiles, $Re_{D_i} = 500$, constant pressure, $H_w = 0{\cdot}04$, ξ to 20.

pressure was taken to be uniform along the tube.

VI. SUMMARY AND CONCLUSIONS

A numerical procedure for the solution of the differential form of the laminar flow equations on a finite difference basis was described and applied to the calculation of a high temperature gas flow through the entrance region of an externally cooled tube.

The predictions were compared to experimental measurements and good agreement was found for the wall heat flux—the important result which governs the cooling requirements and energy loss from the flow—and the internal flow and thermal distributions. The flows considered are characterized by relatively large energy and momentum losses, behaving differently than more familiar laminar flows through tubes with little or no heat transfer. Because of the relatively large energy loss by heat transfer to the wall, the gas decelerates along the tube while cooling and momentum losses are significant due to wall shear forces that retard the flow. Both the velocity and thermal boundary layers grow to the centerline a few diameters downstream of the inlet and the core flow becomes non-adiabatic. The pressure is found experimentally to be nearly uniform along the flow in the entrance region (actually increases slightly) and this is believed to primarily occur because of the negligible mass flux deficit in the shear flow.

Extension of the calculations to a larger range of Reynolds number and Mach number (viscous dissipation) revealed negligible differences in the non-dimensional heat flux Q along tubes in a representation where axial distance was included in the group $\Xi = (z/D)(1/Re_{D_i} Pr)$, which also correlated the experimental measurements.

It would appear that the main features of the numerical method could be employed in subsequent investigations of other aspects of internal flows that are found in practice e.g. variable cross-sectional area channels, a partially ionized gas. Higher Reynolds number flows could also be treated by including turbulent transport of momentum and heat.

ACKNOWLEDGEMENTS

The author expresses his gratitude to Mr. M. Diethelm (of JPL) for programming and carrying out the numerical calculations on a digital computer, and to Mr. P. Massier (of JPL) who supervised the acquisition of the experimental data.

REFERENCES

1. P. F. Massier, L. H. Back and E. L. Roschke, Heat transfer and laminar boundary layer distributions in an internal subsonic gas stream at temperatures up to 13,900 °R, *J. Heat Transfer* **91C**, 83–90 (1969).
2. L. H. Back, Effects of severe surface cooling and heating on the structure of low speed, laminar boundary layer gas flows with constant free-stream velocity, TR 32-1301, Jet Propulsion Laboratory, Pasadena, Calif. (1968).
3. P. M. Worsoe-Schmidt and G. Leppert, Heat transfer and friction for laminar flow of gas in a circular tube at high heating rate. *Int. J. Heat Mass Transfer* **8**, 1281–1301 (1965).
4. R. G. Deissler and A. F. Presler, Analysis of developing laminar flow and heat transfer in a tube for a gas with variable properties, Proc. 3rd Int. Heat Transfer Conf. AICHE, Vol. 1, pp. 250–256 (Aug. 1966).
5. F. P. Incropera and G. Leppert, Laminar flow heat transfer from an argon plasma in a circular tube, *Int. J. Heat Mass Transfer* **10**, 1861–1873 (1967).
6. L. H. Back, Laminar boundary layer heat transfer from a partially ionized monoatomic gas, *Physics Fluids* **10**, 807–819 (1967).
7. P. J. Schneider, Effect of axial fluid conduction on heat transfer in the entrance regions of parallel plates and tubes, Proc. Heat Transfer Fluid Mech. Inst., pp. 41–57 (1956) and *Trans. Am. Soc. Mech. Engrs* **79**, 765–773 (May 1957).
8. Y. L. Wang and P. A. Longwell, Laminar flow in the inlet section of parallel plates, *A.I.Ch.E. Jl* **10**, 323–329 (1964).
9. L. M. Simuni, Motion of a viscous incompressible fluid in a plane pipe, *Vychisl. Mat. Mat. Fiz.* **5**, 1138–1141 (1965). (Translation by Lockheed Missiles & Space Company, Sunnyvale, California, available as NASA-STAR N-66-18422).
10. M. Friedmann, J. Gillis and N. Liron, Laminar flow in a pipe at low and moderate Reynolds numbers, *Appl. Sci. Res.* **19**, 426–438 (1968).
11. E. Baum and M. R. Dennison, Interacting supersonic laminar wake calculations by a finite difference method, *AIAA Jl* **5**, 1224–1230 (1967).
12. J. R. Bodoia and J. F. Osterle, Finite difference analysis of plane Poiseuille and Couette flow developments, *Appl. Sci. Res.* **10A**, 265–276 (1961).
13. R. W. Hornbeck, Laminar flow in the entrance region of a pipe, *Appl. Sci. Res.* **13A**, 224–232 (1964).

14. M. M. WENDEL and S. WHITAKER, Remarks on the paper "Finite difference analysis of plane Poiseuille and Couette flow developments" by J. R. BODOIA and J. F. OSTERLE, *Appl. Sci. Res.* **11A**, 313–317 (1963).
15. C. L. HWANG and L. T. FAN, Finite difference analysis of forced-convection heat transfer in entrance region of a flat rectangular duct, *Appl. Sci. Res.* **13A**, 401–422 (1964).
16. R. W. HORNBECK, An all-numerical method for heat transfer in the inlet of a tube, ASME Paper 65-WA/HT-36 (1965).
17. W. E. MERCER, W. M. PEARCE and J. E. HITCHCOCK, Laminar forced convection in the entrance region between parallel flat plates, *J. Heat Transfer* **89C**, 251–257 (1967).
18. R. MANOHAR, Analysis of laminar-flow heat transfer in the entrance region of circular tubes, *Int. J. Heat Mass Transfer* **12**, 15–22 (1969).
19. E. M. SPARROW, S. H. LIN and T. S. LUNDGREN, Flow development in the hydrodynamic entrance region of tubes and ducts, *Physics Fluids* **7**, 338–347 (1964).
20. W. M. KAYS, Numerical solutions for laminar flow heat transfer in circular tubes, *Trans. Am. Soc. Mech. Engrs* **77**, 1265–1274 (1955).
21. C. A. BANKSTON, The transition from turbulent to laminar gas flow in a heated pipe, *J. Heat Transfer* **92C**, 569–579 (1970).
22. C. A. BANKSTON and D. M. MCELIGOT, Turbulent and laminar heat transfer to gases with varying properties in the entry region of circular ducts, *Int. J. Heat Mass Transfer* **13**, 319–344 (1970).
23. E. J. ROSCHKE, Thermal radiation from ionized argon: results obtained with an annular hohlraum, SPS 37–43, Vol. IV, pp. 206–216 and 222–223, Jet Propulsion Laboratory, Pasadena, California (Feb. 1967).
24. K. W. STARNER and D. J. SPENCER, An arc plasma channel for testing of re-entry boundary layer instrumentation, TR-1001(2240-10)-5, Aerospace Corp., El Segundo, Calif. (Nov. 1966).
25. H. MIRELS, Subsonic flow of hot gas through a highly cooled channel, *AIAA Jl* **6**, 1585–1587 (1968).
26. J. CRANK and P. NICOLSON, A practical method for numerical evaluation of solutions of partial differential equations of the heat-conduction type, *Camb. Phil. Soc. Proc.* **43**, 50–67 (1947).
27. S. V. PATANKAR and D. B. SPALDING, A finite-difference procedure for solving the equations of the two-dimensional boundary layer, *Int. J. Heat Mass Transfer* **10**, 1389–1411 (1967).

APPENDIX A

Finite Difference Formulation

By expressing equations (5) and (6) in finite difference form, the numerical solution can be carried out in the axial direction ξ because of the parabolic nature of the equations. There are a number of ways that finite difference approximations of the derivatives can be written and these are generally obtainable from Taylor series expansions about points in a variable mesh grid (Fig. 13).

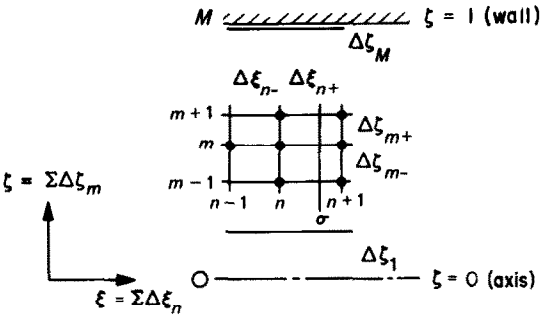

FIG. 13. Grid system.

To obtain the required resolution near the wall as mentioned in the Introduction, a variable radial increment that becomes progressively smaller as the wall is approached was used. In the notation of Fig. 13 the radial increments are given by

$$\Delta\zeta_{m+} = k\Delta\zeta_{m-} = k^m\Delta\zeta_1 \tag{A.1}$$

where the factor $k < 1$. The radial increment adjacent to the wall $\Delta\zeta_M$ can then be expressed in terms of k and the number of increments across the flow M.

$$\Delta\zeta_M = k^{M-1}\left(\frac{1-k}{1-k^M}\right). \tag{A.2}$$

Some values of the radial mesh parameters are given in Table 3 and are later discussed in Appendix C.

Table 3. Radial mesh parameters

$M = 20$			$M = 40$		
$\Delta\zeta_M$	k	$\Delta\zeta_1$	$\Delta\zeta_M$	k	$\Delta\zeta_1$
0·001	0·747	0·254	0·001	0·885	0·116
0·0025	0·792	0·210	0·0025	0·912	0·090
0·005	0·829	0·176	0·005	0·935	0·071
0·01	0·871	0·139	0·01	0·960	0·051

The radial derivatives of a variable were approximated as follows:

$$\left(\frac{\partial f}{\partial\zeta}\right)_m \cong \frac{\Delta f_m}{2(\Delta\zeta_1 k^{m-1})} + 0[(\Delta\zeta_m)^2]\frac{\partial^3 f}{\partial\zeta^3} \tag{A.3}$$

$$\left(\frac{\partial^2 f}{\partial\zeta^2}\right)_m \cong \frac{\Delta^2 f_m}{(\Delta\zeta_1 k^{m-1})^2} + 0[(1-k)\Delta\zeta_m]\frac{\partial^3 f}{\partial\zeta^3} \tag{A.4}$$

where

$$\Delta f_m = \frac{f_{m+1} - (1-k^2)f_m - k^2 f_{m-1}}{\frac{1}{2}(1+k)} \tag{A.5}$$

$$\Delta^2 f_m = \frac{f_{m+1} - (1+k)f_m + kf_{m-1}}{(1/2k)(1+k)} \tag{A.6}$$

For a fixed radial increment, i.e. $k = 1$, these relations reduce to standard central difference formulas. The finite difference approximation of the symmetry condition along the axis $\zeta = 0$ where $\partial f/\partial\zeta = 0$, is

$$\left(\frac{\partial^2 f}{\partial\zeta^2} + \frac{1}{\zeta}\frac{\partial f}{\partial\zeta}\right)_{o,n} = \frac{4}{(\Delta\zeta_1)^2}(f_{1,n} - f_{0,n}) + 0[(\Delta\zeta_1)^2].$$

A variable axial increment was used and axial derivatives were approximated by a three point Lagrangian formula that can also be obtained from Taylor series expansions.

$$\left(\frac{\partial f}{\partial\xi}\right)_{m,n+1} \cong \frac{2\Delta\xi_{n+} + \Delta\xi_{n-}}{\Delta\xi_{n+}(\Delta\xi_{n-} + \Delta\xi_{n+})} f_{m,n+1} - \frac{(\Delta\xi_{n-} + \Delta\xi_{n+})}{\Delta\xi_{n-}\Delta\xi_{n+}} f_{m,n} + \frac{\Delta\xi_{n+}}{\Delta\xi_{n-}(\Delta\xi_{n-} + \Delta\xi_{n+})} f_{m,n-1} + 0[(\Delta\xi_n)^2]\frac{\partial^3 f}{\partial\xi^3}. \quad (A.7)$$

This approximation is more accurate than the forward difference relation

$$\left(\frac{\partial f}{\partial\xi}\right)_{m,n} \cong \frac{f_{m,n+1} - f_{m,n}}{\Delta\xi_{n+}} + 0[\Delta\xi_{n+}]\frac{\partial^2 f}{\partial\xi^2}. \quad (A.8)$$

To attempt to reduce the calculation time, the location at which radial derivatives were evaluated were weighed between the n and the $n + 1$ axial location by the factor σ, i.e. equations (A.3) and (A.4) become

$$\left(\frac{\partial f}{\partial\zeta}\right)_{m,n+\sigma} = (1 - \sigma)\frac{\Delta f_{m,n}}{2(\Delta\zeta_{1,n}k^{m-1})} + \sigma\frac{\Delta f_{m,n+1}}{2(\Delta\zeta_{1,n+1}k^{m-1})} \quad (A.9)$$

$$\left(\frac{\partial^2 f}{\partial\zeta^2}\right)_{m,n+\sigma} = (1 - \sigma)\frac{\Delta^2 f_{m,n}}{(\Delta\zeta_{1,n}k^{m-1})^2} + \sigma\frac{\Delta^2 f_{m,n+1}}{(\Delta\zeta_{1,n+1}k^{m-1})^2}. \quad (A.10)$$

The weighing factor σ should range between $\frac{1}{2}$ and 1—a value of $\frac{1}{2}$ corresponds to the Crank–Nicolson method [26]. Worsoe–Schmidt and Leppert suggest a value of $\frac{3}{4}$, and Patankar and Spalding [27] in a boundary layer calculation use a value of 1. Experience with different values of σ is discussed in Appendix C.

The calculation scheme consists of using equations (5) and (6) to *directly* solve for the axial velocities and total enthalpies across the flow at the $n + 1$ axial location from the known variables at the prior axial locations $n - 1$ and n by a method of successive iterations. The other relations given by equations (8)–(10) are used to express ρ, μ and T in terms of w and H_t. The radial velocities are obtained by integration of the continuity equation

$$u = -\frac{1}{\rho\zeta}\int_0^\zeta \frac{\partial(\rho w)}{\partial\xi}\zeta d\zeta \quad (A.11)$$

with a backward difference used for the ξ-derivative. To retain the simple calculation form of the explicit method whereby values of w and H_t at the $n + 1$ location, denoted by $f_{m,n+1}$, can be directly obtained from the left side of equations (5) and (6), a different scheme than normally used was chosen to solve the implicit form of the equations considered herein. The scheme consists simply of evaluating the terms on the right side of equations (5) and (6) from the jth iteration to obtain the $j + 1$ iterate directly from the left side of the equations. In functional form the procedure is given by

$$\left(\frac{\partial f}{\partial\xi}\right)^{j+1}_{m,n} = g\left[f^j_{m,n+\sigma}; \left(\frac{\partial f}{\partial\zeta}\right)^j_{m,n+\sigma}; \left(\frac{\partial^2 f}{\partial\zeta^2}\right)^j_{m,n+\sigma}\right]. \quad (A.12)$$

For example, for a forward difference in the axial direction

$$\left(\frac{\partial f}{\partial\xi}\right)^{j+1}_{m,n} = \frac{f^{j+1}_{m,n+1} - f_{m,n}}{\Delta\xi_n} \quad (A.13)$$

and a similar expression follows for the three point relation equation (A.7). The term $f^j_{m,n+\sigma}$ is given by

$$f^j_{m,n+\sigma} = (1 - \sigma) f_{m,n} + \sigma f^j_{m,n+1} \quad (A.14)$$

with similar expressions for the radial derivatives equations (A.9) and (A.10), i.e. where $\Delta f_{m,n+1}$ and $\Delta^2 f_{m,n+1}$ are jth iterate terms. This scheme avoids obtaining a solution of the system of $2M$ algebraic equations by matrix inversion that arises in the implicit method after the non-linear algebraic equations are linearized and which system also must be iterated because of the approximate linearized form of the equations that are solved.

In carrying out the calculations the values of w, H_t and u in the iteration scheme are taken to be average values between the $j + 1$ and jth iterations to avoid overcorrections,

$$f^{j+1}_{m,n+1} = \tfrac{1}{2}[(f^{j+1}_{m,n+1})_{\text{computed}} + f^j_{m,n+1}]$$

and for the first iteration, an average value between the $n + 1$ and n locations is used

$$f_{m,n+1} = \tfrac{1}{2}[(f_{m,n+1})_{\text{computed}} + f_{m,n}].$$

To start the iteration scheme values of w and H_t at the $n + 1$ location are obtained by projecting the history of the flow downstream through linear extrapolation from the prior $n - 1$ and n locations. The iteration scheme is continued until all the variables converge to within some specified tolerance ϵ, i.e.

$$\left|\frac{f^{j+1}}{f^j} - 1\right| < \epsilon \quad (A.15)$$

or when a variable is very small, $|f^{j+1} - f^j| < \epsilon$. The calculation then proceeds to the next axial location.

The input parameters are γ, M_i, Pr, ω, Re_i, the initial profiles $w(\zeta)$ and $H_t(\zeta)$ and either w'_i or H'_{t_i}, and the thermal boundary condition $H_w(\xi)$ and pressure distribution $p(\xi)$ along the wall for the case where p is prescribed. Specifica-

Table 4. Information on numerical calculation parameters

Condition	M No. of radial increments	$\Delta\zeta_M$ Radial increment at wall	$\Delta\xi$ Axial increment	ϵ Tolerance on iteration convergence	J No. of iterations at each axial step	σ Weighing factor	Computation time
Tests 51-H, 59-H, 63-H $H_w = 0{\cdot}04$	Used 40. Profile slopes at wall and integrals less accurate with $M = 20$. Profile slopes at wall could be 10% in error for $M = 20$	(1) For severe cooling $H_w \to 0$, $\Delta\zeta_M = 0{\cdot}0025$ gave best overall results in terms of accuracy and computation time. (2) Could not get started with $\Delta\zeta_M$ less than 0·0025 *or needed* abnormally large number of axial steps. (3) For larger $\Delta\zeta_M$ profile slopes less accurate.	(1) 100 steps each at successively increasing values of $\Delta\xi = 0{\cdot}001$, 0·0015, 0·002, 0·0025, 0·003 and 0·0035. Then 3430 steps at $\Delta\xi = 0{\cdot}004$. Total 4030 steps. (2) Usually could not start with $\Delta\xi \geqslant 0{\cdot}002$ (too large) (3) Smaller $\Delta\zeta_M$, smaller $\Delta\xi$ required. (4) Could increase $\Delta\xi$ along tube but number of iterations increase and computation time increases.	10^{-3} Smaller tolerance 10^{-8} negligibly changed results, but computation time increased significantly.	5 at most usually 1 or 2	Used 1 Tried $\frac{1}{2}$, $\frac{3}{4}$ and 1, hardly any difference in accuracy or computation time.	Test 51-H—22 min 59-H— 9 min 63-H—23 min
Pressure calculated Test 51-H	40	0·0025	Same as Test 51-H above	10^{-3}	5 at most, usually 2 or 3	1	Almost twice as long as for constant pressure calculation
Effect of increasing Re_D $H_w = 0{\cdot}04$	40	0·0025	Could increase, recall stability requirement, $\Delta\xi \propto (\Delta\zeta)^2\, Re$ for idealized flow and $\Delta\zeta$ = constant	10^{-3}	3 at most, usually 1	1	$Re_D =$ 500–13 min 1000–9 min 2000–9 min
Effect of increasing Mach number $H_w = 0{\cdot}04$	40	0·0025	Same as Test 51-H above	10^{-3}	8 at most, usually 2 for $M_i = 0{\cdot}75$, more iterations increased computation time.	1	$M_1 = 0{\cdot}1$ –13 min 0·75–42 min

tion of γ and M_i, determines P and K from equation (7). Since the definition of total enthalpy was used in expressing K in the form of equation (7), it is necessary to specify either w_i' or H_{t_i}' (H_{t_i}' was used) to be able to calculate the remaining initial quantities w_i', T_i', p_i', ρ_i' *and* μ_i' from the definitions of P, K and Re_i, equation (7), and equations (8) and (9). Values of c_{p_i}' and $\mu_i'(T_i')$ are also needed for a particular gas.

The heat flux to the wall and the shear stress at the wall were obtained from the following expressions

$$q_w' = -k_w'\left(\frac{\partial T'}{\partial r}\right)_w = -\frac{k_w' H_{t_i}'}{r_w c_{p_w}'}\left(\frac{\partial H_t}{\partial \zeta}\right)_w$$

$$\tau_w' = \mu_w'\left(\frac{\partial w'}{\partial r}\right)_w = \frac{\mu_w' w_i'}{r_w}\left(\frac{\partial w}{\partial \zeta}\right)_w.$$

The slopes of the enthalpy and velocity profiles at the wall were established by extrapolating a parabola from the three points nearest the wall to a point halfway between the wall and the first point away from the wall. A cubic was then fit through the first two points away from the wall, the extrapolated point and the point on the wall; and from this curve fit the slope of the profiles at the wall was determined. Even with the small radial mesh size near the wall it was necessary to use this extrapolation procedure to obtain accurate heat fluxes and shear stresses; smaller radial increments yet near the wall resulted in smaller axial increments and thus longer computation time.

APPENDIX B

Other Numerical Approaches Attempted

As mentioned in Section III an attempt was made to satisfy all of the global conservation equations (14), (16) and (17) at each axial step by calculating new values of ρ, w and H_t across the flow after each iteration from the following relations corresponding to conserving mass, momentum and energy

$$(\rho w)_{\text{corrected}} = (\rho w)_{\text{computed}} \frac{I_{m_i}}{(I_m)_{\text{computed}}}$$

$$(\rho w^2)_{\text{corrected}} = (\rho w^2)_{\text{computed}} \frac{(I_M)_{\text{momentum balance equation (16)}}}{(I_M)_{\text{computed}}}$$

$$(\rho w H_t)_{\text{corrected}} = (\rho w H_t)_{\text{computed}} \frac{(I_H)_{\text{energy balance equation (17)}}}{(I_H)_{\text{computed}}}.$$

Knowing ρ, w and H_t from these three relations, the other variables could be calculated. The calculated pressure then varies radially across the flow as well as along the flow. An attempt to calculate an average pressure across the flow

$$\bar{p} = 2\int_0^1 p\zeta \, d\zeta$$

led to diverging values of $\bar{p}$ as the iteration proceeded at an axial location.

An effort was made to calculate the pressure distribution along the flow by using only the mass flow constraint, as has been done by others (Section III), but this method also failed for the high temperature flows considered. The application herein involved substituting the density from the equation of state into the mass flow constraint, and trying to adjust $p(z)$ to satisfy the mass flow constraint in subsequent iterations. This method diverged.

Deissler and Presler's method (Section III) was also tried, i.e. applying the momentum equation at the wall to specify the pressure. This method produced reasonable results for a nearly constant property flow as was also found by Deissler and Presler. However, the method failed with appreciable wall cooling because a significant increase in wall pressure was predicted whereas none was observed experimentally. In the prediction a uniform radial increment was used. The method was not tried with variable radial mesh spacing.

APPENDIX C

Numerical Calculation Parameters

A description of the values of the numerical parameters that were used in the uniform pressure calculations is contained in Table 4 along with comments pertaining to the interrelation between the parameters. The numerical values noted reflect much trial and error experience for which the actual computation time was considerably greater than those times shown for the final calculations. A UNIVAC 1108 computer was used in the calculations.

ECOULEMENT LAMINAIRE À TRÈS HAUTE TEMPÉRATURE D'UN GAZ À TRAVERS LA RÉGION D'ENTRÉE D'UN TUBE REFROIDI CALCULS NUMÉRIQUES ET RÉSULTATS EXPÉRIMENTAUX

Résumé—On résout numériquement sur calculateur digital les équations aux dérivées partielles de l'écoulement laminaire d'un gaz à très haute température à travers la région d'entrée d'un tube refroidi extérieurement. On décrit la méthode de résolution et les calculs sont menés en relation avec les mesures experimentales. Les résultats indiquent des pertes relativement grandes d'énergie et de quantité de mouvement dans les écoulements fortement refroidis où la pression est presque uniforme le long de l'écoulement et où l'écoulement du noyau devient non adiabatique quelques diamètres en aval de l'entrée, ce qui est en bon accord avec l'expérience. On étudie aussi les effets d'un large domaine du nombre de Reynolds et du nombre de Mach (dissipation visqueuse).

LAMINARE STRÖMUNG EINES GASES MIT SEHR HOHER TEMPERATUR DURCH DAS EINTRITTSGEBIET EINES GEKÜHLTEN ROHRES.

NUMERISCHE BERECHNUNG UND EXPERIMENTELLE ERGEBNISSE

Zusammenfassung—Die Gleichungen in differentieller Form für die laminare Strömung eines Gases mit sehr hoher Temperatur durch den Eintrittsbereich eines aussen gekühlten Rohres wurden numerisch mittels eines Digitalrechners gelöst. Die Lösungsmethode wurde beschrieben und Berechnungen zusammen mit experimentellen Messungen durchgeführt. Die Übereinstimmung mit dem Experiment ist gut; das Ergebnis zeigt einen relativ hohen Energie- und Impulsverlust in der betrachteten, stark gekühlten Strömung, wo der Druck entlang der Strömung fast konstant bleibt und der Strömungskern um einige Durchmesser strömungsabwärts vom Eintritt nicht adiabat wird. Die Einflüsse eines grossen Bereichs der Reynolds- und Machzahlen (viskose Auflösung) wurden ebenfalls untersucht.

ЛАМИНАРНОЕ ТЕЧЕНИЕ СИЛЬНО НАГРЕТОГО ГАЗА ЧЕРЕЗ ВХОДНОЙ УЧАСТОК ХОЛОДНОЙ ТРУБЫ. ЧИСЛЕННЫЕ РАСЧЁТЫ И ЭКСПЕРИМЕНТАЛЬНЫЕ РЕЗУЛЬТАТЫ

Аннотация—Численно решена система дифференциальных уравнений, описывающих ламинарное течение сильно нагретого газа во входном участке охлаждаемой снаружи трубы. Описан метод решения. Одновременно с расчётами проводились экспериментальные измерения. Получено хорошее согласие теоретических и экспериментальных данных. Результат анализа свидетельствует об относительно больших потерях энергии и количества движения сильно охлажденных потоков, в которых давление почти постоянно вдоль потока, а ядро потока становится неадиабатичным на расстоянии нескольких диаметров от входа. Исследовался широкий диапазон чисел Рейнольдса и Маха (вязкая диссипация).